Doppler Characterization in Ultra Wideband BAN Channels During Breathing

Ruben-Gregorio Garcia-Serna, Member, *IEEE*, Concepcion Garcia-Pardo, Jose-Maria Molina-Garcia-Pardo, Leandro Juan-Llacer, Senior Member, *IEEE*, and Narcis Cardona

Abstract—**Monitoring physical parameters from devices inside the body using Ultra Wideband (UWB) technology, enables the development of high bandwidth demanding applications at real time. The relative movement of the nodes deployed in the body due to breathing, can give rise to a frequency shifting effect, increasing the fading level in the propagation channel during transmissions. In this article, therefore, we present a study of the frequency effects on the propagation channel derived from the relative movement between two nodes of a wireless body area network (WBAN), at least one of them placed inside the human body, caused by breathing. The study is performed on the basis of the Doppler spectrum characterization in terms of the shape fitting and the frequency spread parameters derivation. Continuous wave (CW) signals have been used to cover the UWB range at four selected frequencies: 3.1 GHz, 4.8 GHz, 6 GHz and 8.5 GHz, and a liquid phantom has been employed for emulating the dielectric properties of the high water content tissues at the considered UWB frequencies.**

Index Terms—**Doppler, Body Area Networks, channel characterization, UWB, implant communications, breathing.**

I. INTRODUCTION

RESEARCH on smart medical implants in areas like sensors, biocompatible materials, antennas design, energy harvesting techniques and efficient communication systems, just to name a few, is bringing new ways of expanding the human medical monitoring concept [1]-[3]. Prevention and early detection of diseases as well as unattended treatments delivery will be a central element in future medicine, in order to improve the available medical resources and the patients' quality of life [4].

The deployment of implanted devices implies the transmission of signals throughout the human body tissues. However, the human body imposes severe conditions to the propagation of radio signals transmitted from devices

placed inside due to the high propagation losses as well as the inherent heterogeneous nature of the living tissues [5]. This condition restricts the feasible frequency bands and, as a consequence, the available bandwidth for applications.

Despite the IEEE 802.15.6-2012 standard for Body Area Networks (BAN) proposes the Medical Implants Communications Services (MICS) 402 MHz to 405 MHz band for the communication with implants [6], other bands as the ultra wideband (UWB) one, from 3.1 GHz to 10.6 GHz, have been under intense research for short-range radio interconnection links, with the aim of enhancing the narrow maximum bandwidth of 300 kHz available in the MICS band [7]-[10]. The application of UWB in scenarios demanding high data rates, like video transmission from wireless endoscopy capsules, has been under research in the last few years [11]-[13].

Depending on the relative position between communication nodes, considering at least one of them inside the body, three types of propagation channels can be identified as: in-body to in-body (IB2IB), in-body to on-body (IB2OB) and in-body to off-body (IB2OFF). The relative position between any of these communication pairs, transmitter (Tx) or receiver (Rx), can change during the transmission time giving rise to a displacement on the carrier frequency f_c or Doppler effect in the received signal. In absence of any external body position change, the main source of this motion could be associated to breathing.

During inspiration, the diaphragm contracts moving down from 1-2 cm (quite breathing conditions) to 10-12 cm (forced breathing) compressing the upper abdominal organs at the same time the vertical dimension of the chest cavity increases [14]. The lateral and anteroposterior dimension of the thorax increases due to the contraction of the external intercostal muscles and the ribs movement. This produces an expansion of the chest typically ranging from 3 cm to 10 cm [15]. Besides, as the lungs get inflated, they fill the thoracic cavity causing a displacement and rotation of the heart [16]. The expiration, basically passive during quite breathing, returns the lungs and chest wall to its resting position. The inspiration-expiration cycle is repeated from 12 to 18 times per minute, increasing up to 50 times per minute during exercise [17].

The number of studies addressing the effects of the human breathing in the communication channel is very limited in the literature [18]. The best of the authors' knowledge, there is not any previous study of the Doppler effect caused by the human

Ruben-Gregorio Garcia-Serna, Jose-Maria. Molina-Garcia-Pardo and Leandro Juan-Llacer are with the Information Technologies and Communications Department, Universidad Politecnica de Cartagena, Cartagena 30202, Spain (e-mail: josemaria.molina@upct.es, rugarser@gmail.com, leandro.juan@upct.es).

Concepcion Garcia-Pardo and Narcis Cardona are with the iTEAM research institute, Universitat Politècnica de València, 46022 Valencia, Spain (e-mail: cgpardo@iteam.upv.es; ncardona@iteam.upv.es).

breathing in the in-body channel applied to BANs at UWB frequencies. Thus, the main contribution of this paper is the quantification of the Doppler effect caused by the relative motion between communication nodes during breathing, considering at least one of them placed inside the body. The study was performed using continuous wave (CW) signals in the UWB range and the in vivo conditions were emulated using a liquid phantom with dielectric characteristics similar to the human high water content tissues, at the considered band.

This paper is organized as follows. The description of the elements involved in the measurement of the channel frequency responses is carried out in Section II. Section III defines the basic parameters used in the analysis of the measured data in the frequency domain. Data processing methodology upon the defined frequency parameters is described in Section IV. In Section V a theoretical time domain model for the breathing process is derived. Section VI describes the characterization of the considered time-variant channels in frequency. Finally, the main conclusions of the research are presented in Section VII.

II. MEASUREMENTS SETUP

A. Measurement Elements Characteristics

Performing in vivo measurement in humans is neither frequently available nor ethically accepted and usually can be emulated using phantom materials with electrical properties similar to a considered body tissue at a particular frequency.

During this research, the thoracic cavity of a human being was simulated using an expanded polystyrene (EPS) foam container of external dimensions $28 \times 28 \times 28$ cm^3 and walls with 4 cm thickness. The container was filled with a liquid phantom designed to emulate the dielectric properties of the high water content tissues of the body (as muscles) at ultra wideband (UWB) frequencies from 3.1 GHz to 10.6 GHz. This phantom was formulated as a sucrose based solution ($C_{12}H_{22}O_{11}$, 1.0 mol/l), as described in [19]. The real part of the complex permittivity ε_r within the operation band was reported to present a variation from 30 to 50 at 25 ºC. The system lungs-trachea was implemented using an inflatable natural rubber latex sphere immersed in the phantom and connected to a 96 cm corrugated tube with a valve at the end. This valve allowed a manual insertion of air into the sphere at the same time it prevented the insufflated air from escaping unintentionally. Attached to the rubber sphere was mounted a planar antenna of dimensions 5×4.4 cm [20] used as transmitter (Tx). In order to avoid short-circuiting, the antenna immersed in the phantom was first covered with a latex rubber material of relative permittivity ε_r similar to the air. The connection between Tx and the sphere was performed using adhesive tape. Therefore, the ensemble allowed us to emulate the movement of a transmitter device during breathing and to analyze the effect on the radio propagation channel.

The placement position of a planar receiver antenna (Rx), with the same characteristics as Tx, was selected depending on the channel type under consideration as depicted in Fig. 1. The

order of the measurements was arranged to consider first the most usual communication channels (IB2OB and IB2OFF), like in capsule endoscopy applications, and in the end, the IB2IB channel between two implanted nodes. Thus, during the IB2OB radio channel Doppler characterization Rx was fixed on the external side of the container facing Tx. The separation distance between Tx and Rx ranged from 13 cm for the resting position to 9 cm for the maximum Tx expansion. During the IB2OFF radio channel characterization Rx was placed out of the container at 4 separation distances: 10 cm, 20 cm, 30 cm and 50 cm. Finally, for the IB2IB channel characterization, Rx was first covered with the same latex rubber material used for Tx and immersed in the phantom. Both antennas were located at 7 cm from each other.
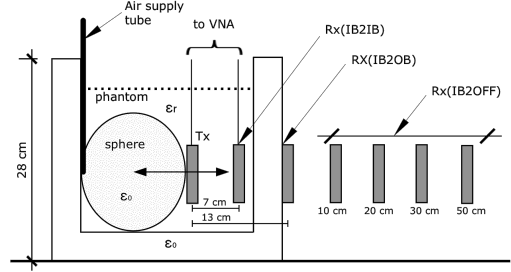

Fig. 1. Measurement elements setup.

B. Channel Sounder

The $S_{21}(f_c, t)$ scattering parameter, representing the time-varying complex frequency response $H(f_c, t)$ of the channel for each channel configuration (IB2OB, IB2OFF and IB2IB) at the central frequency f_c and time t was measured using a Vector Network Analyzer (VNA) model Agilent ENA E5072A controlled using a custom software developed in Matlab$^©$.

The VNA was configured to transmit a CW sinusoidal signal at a single frequency f_c with a sampling time of 133 samp/seg. This configuration allows measuring a maximum Doppler shift f_m of 66 Hz, enough for the current application. The noise floor of the measurements for the VNA configuration was kept below -105 dB. The detailed setup parameters of the VNA are listed in Table I. The maximum shifting distance between Tx and Rx was restricted to 4 cm to emulate a normal chest expansion during quite breathing conditions [15].

TABLE I
VNA SETUP PARAMETERS

IF	10 kHz
Span	0 Hz (Continuous Wave)
Sweep Time	60 s
Nº Points	8005
Tx Power	5 dBm
f_c	3.1 GHz, 4.8 GHz, 6 GHz and 8.5 GHz

III. Frequency Parameters Derivation

A. Radio Channel Frequency Dispersion

The characterization of the channel Doppler frequency shift caused by the relative motion between Tx and Rx because of breathing was carried out from the measured $S_{21}(f_c,t) = H(f_c,t)$ scattering parameter of the channel when transmitting an unmodulated CW signal $s(t) = \Re\{e^{j(2\pi f_c t + \phi_0)}\}$ of central frequency f_c. Due to the motion of Tx with respect to Rx, the received signal exhibits a deviation from f_c, or Doppler effect. This frequency shift ρ, for a single frequency $(\Delta f = 0)$, can be described in terms of the Doppler power spectrum function $D(f_c,\rho)$ obtained as the Fourier transformation (FT) of the channel autocorrelation function $R_H(\Delta f = 0, \Delta t)$ with respect to Δt as [21]

$$D(f_c,\rho) = \int R_H(\Delta f = 0, \Delta t) \cdot e^{-j2\pi\rho\Delta t}\, d\Delta t \qquad (1)$$

As the FT of the autocorrelation of a time series is equivalent to the squared magnitude of the FT of the original series [21], we can calculate the Doppler power spectrum at a frequency f_c as

$$D(f_c,\rho) = \left| \mathcal{F}\{H(f_c,t)\} \right|^2 \qquad (2)$$

From the Doppler power spectrum function two parameters of interest can be derived to describe the frequency dispersive behavior of the radio channel: the Doppler spread B_D, defined as the frequencies range where the value of $D(f_c,\rho)$ is above a fixed threshold [22], and the Root Mean Square (RMS) Doppler spread [21], calculated as the second order moment of the spectrum as

$$\rho_{RMS} = \sqrt[2]{\frac{\int \rho^2 D(f_c,\rho)\,d\rho}{\int D(f_c,\rho)\,d\rho}} \qquad (3)$$

IV. Data Processing

The study of the Doppler effect caused by the movement between two antennas, at least one of them inside the body, during breathing was quantified in the frequency domain in terms of the Doppler spread B_D and the RMS Doppler Spread ρ_{RMS}. Theoretical values of B_D considering breathing as a perfect sinusoidal process at the same rate of each measured one for a 4 cm maximum expansion were first calculated as reference (B_{Dref}) in all the considered scenarios. This enabled us to verify how close are the measured values with respect to the theoretical ones, when the breathing rate keeps constant during the considered time interval. In order to include the variation of the propagation speed in the phantom, the value of ε_r for each considered frequency was taken into account in the theoretical derivation. Reference values of B_D for quite breathing conditions (12 breaths per minute) along with the values of ε_r reported in [19] for each value of f_c are listed in Table II. As shown, the maximum value of B_{Dref} is below 6 Hz for the considered ideal conditions.

TABLE II
THEORETICAL DOPPLER SPREAD REFERENCE VALUES

f_c (GHz)	ε_r	B_{Dref} (Hz)
3.1	59	2.54
4.8	53	3.73
6	49	4.48
8.5	41	5.81

At processing stage, each channel frequency response $H(f_c,t)$ was first smoothed to reduce the noise using a moving average filter [23]. This filter has a frequency response of magnitude $|H(\hat{\omega})|$ as

$$|H(\hat{\omega})| = \left| \frac{\sin(\hat{\omega}L/2)}{L\sin(\hat{\omega}/2)} \right| \qquad (4)$$

where $\hat{\omega} = 2\pi f / f_s$, being f_s the sampling frequency. A window size L=20 was selected as a trade-off between frequency resolution and smoothing level considering that the Doppler power spectrum has the energy concentrated within a bandwidth of 6 Hz for the breathing conditions. This way, the cutoff frequency of the filter encloses the considered band as depicted in Fig. 2, with a noise reduction level $\sqrt{L} \approx 4.5dB$.
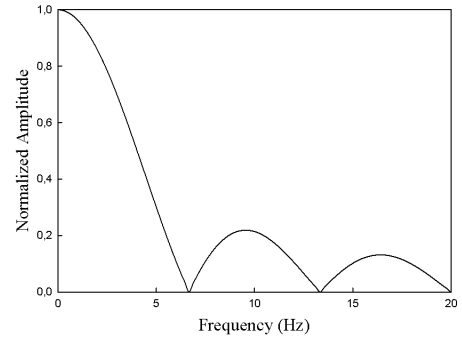

Fig. 2. Moving average filter frequency response positive side magnitude for a window size of 20.

After the noise reduction stage, the Doppler power spectrum was calculated using (2). From $D(f_c,\rho)$, B_D for a threshold value of -35 dB below the zero normalized peak value and ρ_{RMS} parameters were derived.

Due to the reception of multipath components is not angular equispaced and the existence of a dominant LoS component, the shape of $D(f_c,\rho)$ does not exhibit the typical Jake's model bathtub shape. Instead, a symmetrical bell-shape decaying function with a maximum at 0 Hz is formed. In order to obtain a mathematical model of the Doppler spectrum shape a fitting procedure was carried out on the basis of three functions, selected for their continuity and existence in the range of $-\infty < x < +\infty$:

1) Normal

$$\bar{D}(f_c,\rho) = \frac{1}{\sqrt{2\pi\sigma^2}} e^{\frac{-(\rho-\mu)^2}{2\sigma^2}} \tag{5}$$

2) Cauchy

$$\bar{D}(f_c,\rho) = \left(\frac{\lambda}{\pi}\right)\frac{1}{\lambda^2+(\rho-\alpha)^2} \tag{6}$$

3) Laplace

$$\bar{D}(f_c,\rho) = \frac{1}{2s} e^{-\left|\frac{\rho-\alpha}{s}\right|} \tag{7}$$

where μ is the mean, σ is the standard deviation, λ and s are scale factors and α is the position of the maximum of the function.

The goodness of fit between the real function and the estimated one was evaluated using the minimization of the Root Mean Squared Error (RMSE) criterion defined as

$$RMSE = \frac{1}{n}\sqrt{\sum_{i=1}^{n}\left(D_i(f_c,\rho)-\bar{D}_i(f_c,\rho)\right)^2} \tag{8}$$

where $D_i(f_c,\rho)-\bar{D}_i(f_c,\rho)$ is the difference between the i-esime sample of the real function and the estimated one.

V. BREATHING PROCESS MODELING

Because of the periodic nature of breathing, the amplitude variation of the received signal will be periodic as well. Under ideal conditions, the received signal would exhibit a sinusoidal pattern with a single central frequency value proportional to the breathing rate and constant amplitude. In real conditions, the frequency dependence of the inhomogeneous human tissues affects the received signal causing a reduction in the mean power and distortion.

In order to derive a simplified theoretical model for the breathing process, the time variation of the received signal amplitude for a single value of f_c can be described as

$$\bar{H}(f_c,t) = A + \gamma\sin(2\pi\beta t+\varphi) \tag{9}$$

Where:
- A represents the mean received power in dBm.
- γ represents the maximum excursion of the oscillatory process around the mean value.
- β represents the breathing rate (BR) expressed in breaths per minute $(\beta = BR/60)$.
- φ represents the initial phase offset in radians.

The A parameter is related to the static channel response at f_c. The γ parameter depends on the breathing depth, the channel response at the considered frequency and the multipath behavior. It can be obtained by visual inspection as half the mean peak-to-peak value for each measured $H(f_c,t)$. Finally, φ can be obtained by fitting. As in the Doppler spectrum shape fitting, the selected goodness of fit criterion was the RMSE one using (8). In Fig. 3 is depicted the model derived using (9) for the IB2OB channel compared to measured values of $H(f_c,t)$.
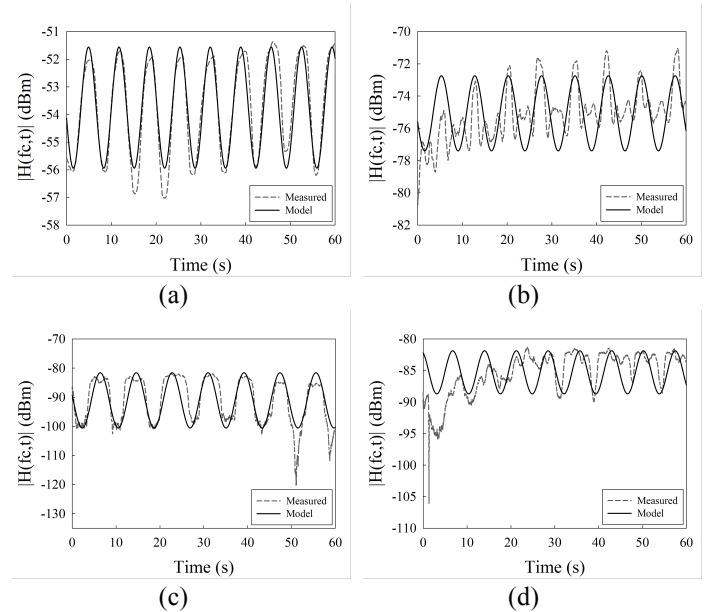
Fig. 3. Measured values of $H(f_c,t)$ for the IB2OB channel. (a) 3.1 GHz, (b) 4.8 GHz, (c) 6 GHz and (d) 8.5 GHz.

From the described model of breathing, it is possible to obtain the theoretical maximum Doppler frequency shift as

$$f_m \approx \frac{vf_c}{c/\sqrt{\varepsilon'_r}} \tag{10}$$

where v is the relative speed between Tx and Rx, f_c is the operation frequency, c is the speed of light and ε'_r is the real part of the permittivity in the propagation medium at the considered frequency. Considering a maximum expansion

of 4 cm (for a chest excursion limit from 3 cm to 10 cm), v can be derived from the relationship between the expansion range and the expansion time calculated as half of the oscillatory process period for each measurement as $v = 4 \cdot 10^{-2} \cdot (2\beta)$. From f_m, the theoretical Doppler spread can be calculated as

$$B_D = 2 \bullet f_m \qquad (11)$$

As the model only considers a single central frequency, the theoretical value derived for B_D can differ from the measured one when the breathing rate does not keep constant during the considered interval.

A. IB2OB Radio Channel Model Parameters

The breathing model parameters after fitting the measured time-varying frequency responses for the IB2OB channel at the selected frequencies are listed in Table III.

TABLE III
MEASURED IB2OB BREATHING MODEL PARAMETERS

f_c (GHz)	A	γ	β	φ	RMSE
3.1	-53.75	2.19	0.147	3.19	0.60
4.8	-75.07	2.33	0.134	3.48	1.46
6	-91.08	9.49	0.122	2.72	2.50
8.5	-85.29	3.41	0.117	1.54	2.51

As it can be observed, the propagation losses get increased with the frequency. Thus, the mean received signal power (parameter A) gets reduced accordingly. An exception is found in the 6-8 GHz band where the IB2OB channel presented an attenuation greater than the surrounding frequencies. Conversely, because the parameter γ depends on the depth of breathing, no dependency with the frequency is found.

B. IB2OFF Radio Channel Model Parameters

The model fitting parameters for the IB2OFF channel at each one of the considered distances are listed in Table IV. The same observations carried out for the IB2OB channel breathing process modeling applies to the IB2OFF scenario.

The variation of the A model parameter with the distance is found to be higher with the frequency than with the distance, as seen in Table IV. This effect can be justified because part of the propagation takes place inside the liquid phantom with higher frequency dependent losses than the air. So the propagation outside the container, for the considered distances, do not affect in a significant way in terms of propagation losses.

TABLE IV
MEASURED IB2OFF BREATHING MODEL PARAMETERS

Off-body distance (cm)	f_c (GHz)	A	γ	β	φ	RMSE
10	3.1	-56.63	1.77	0.100	2.51	0.46
	4.8	-73.71	5.3	0.117	-2.52	1.65
	6	-84.59	2.68	0.117	2.39	1.27
	8.5	-86.59	1.72	0.100	-2.29	0.68
20	3.1	-54.73	0.67	0.100	-2.19	0.24
	4.8	-68.49	0.77	0.133	-2.03	0.27
	6	-84.97	6.43	0.117	-1.29	1.49
	8.5	-90.69	2.01	0.117	2.44	1.0
30	3.1	-54.13	0.79	0.117	-1.06	0.44
	4.8	-70.99	1.59	0.133	0.71	1.33
	6	-85.34	2.89	0.117	-1.89	2.57
	8.5	-89.74	2.57	0.133	1.71	1.07
50	3.1	-57.21	1.82	0.133	1.28	0.43
	4.8	-69.41	0.99	0.133	-0.39	0.50
	6	-84.49	3.38	0.133	1.97	2.07
	8.5	-88.43	1.68	0.133	0.89	0.94

C. IB2IB Radio Channel Model Parameters

Finally, the model parameters for the breathing process in the IB2IB channel is presented in Table V.

TABLE V
MEASURED IB2IB BREATHING MODEL PARAMETERS

f_c (GHz)	A	γ	β	φ	RMSE
3.1	-59.59	5.86	0.200	-2.80	1.97
4.8	-93.02	6.66	0.217	-0.43	3.70
6	-101.1	12.97	0.200	3.28	7.1
8.5	-	-	-	-	-

For the IB2IB channel, the only two feasible frequencies are 3.1 GHz and 4.8 GHz because the mean received power falls below the noise level for the rest of considered frequencies. Besides, this power is observed to present a steeper transition between frequencies (33.4 dBm from 3.1 GHz to 4.8 GHz), compared to the rest of propagation scenarios.

VI. FREQUENCY RADIO CHANNEL CHARACTERIZATION

A. IB2OB Radio Channel

Because of the geometry, the propagation phenomenon was carried out through two media (phantom + container wall) with different values of ε_r, being the second one similar to the air (ε_0). The inflatable sphere also presented a transition from ε_r to ε_0 probably affecting the multipath propagation inside the container.

The Doppler spectrums were obtained from the FT of each measured $H(f_c, t)$ using (2). In Fig. 4 is depicted each one of the Doppler spectrums, for the considered values of f_c, normalized to 0 dB.

The Doppler parameters B_D and ρ_{RMS} obtained from the measured $H(f_c,t)$ are listed in Table VI. In order to evaluate the measured values of B_D, theoretical reference values were first calculated using (10) and (11), and the derived model parameters from Tables III and V. The difference between measured and theoretical values are denoted as ΔB_{Dref} and also included in Table VI. Negative values represent a measured B_D lower than the reference one.
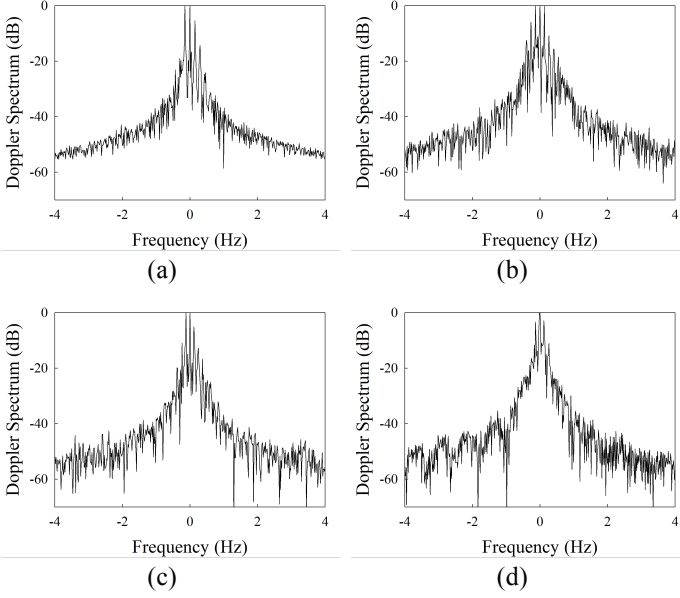

Fig. 4. Measured IB2OB Doppler Spectrum. (a) 3.1 GHz, (b) 4.8 GHz, (c) 6 GHz and (d) 8.5 GHz.

TABLE VI
MEASURED IB2OB CHANNEL DOPPLER PARAMETERS

f_c (GHz)	B_D (Hz)	ΔB_{Dref} (Hz)	ρ_{RMS} (Hz)
3.1	1.63	-0.27	0.44
4.8	2.37	-0.11	0.65
6	1.63	-0.99	0.48
8.5	1.78	-1.62	0.53

As frequency increases, the fading in the channel gets more severe, causing the amplitude of the received signal to change quicker in time as depicted in Fig. 3. This behavior produces a broadening of the signal spectrum. From Table VI, as the frequency increases the measured values of B_D get lower than the theoretical ones, with a maximum difference of 1.62 Hz for 8.5 GHz. This can be explained from the fact that, because of the geometry, not all the space between Tx and Rx is filled with liquid phantom and the period of the real process is not constant during the measurement interval. With the exception of 8.5 GHz, the theoretical values of B_D present a difference lower than 1 Hz respect the measured ones.

The shape of the time-variant IB2OB channel Doppler spectrum was evaluated to find the best fitting model. In Table VII the derived model parameters for the three considered fitting functions (Normal, Cauchy and Laplace) are listed. In addition, the RMSE goodness of fit criterion value, calculated using (8), is included in Table VIII.

TABLE VII
IB2OB DOPPLER SPECTRUM SHAPE FITTING PARAMETERS

f_c (GHz)	Normal		Cauchy		Laplace	
	μ	σ	λ	α	s	α
3.1	-0.012	0.682	0.589	-0.013	0.826	-0.014
4.8	0.015	0.806	0.589	-0.021	0.796	-0.023
6	0.018	0.711	0.637	0.021	0.881	0.006
8.5	0.011	0.611	0.548	0.003	0.758	0.001

TABLE VIII
IB2OB DOPPLER SPECTRUM SHAPE FITTING RMSE VALUES

f_c (GHz)	Normal	Cauchy	Laplace
3.1	0.072	0.066	0.063
4.8	0.082	0.086	0.081
6	0.074	0.071	0.069
8.5	0.082	0.078	0.076

As observed, the function that better fits the shape of the Doppler spectrum is the Laplace one. In general, the Normal function seems to present a less suitable fitting compared to the others as it can be observed in Fig. 5 for 3.1 GHz.
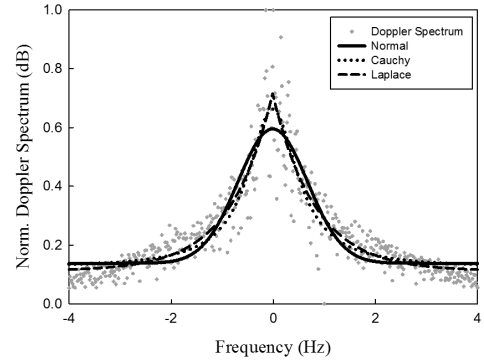

Fig. 5. Doppler spectrum shape fitting for 3.1 GHz.

B. IB2OFF Radio Channel

Values for the derived Doppler parameters for each off-body disposition are listed in Table IX.

As in the IB2OB scenario, the theoretical calculated Doppler spread presents an absolute difference lower than 1 Hz with respect to the measured one. Higher differences were found to relate to slight breathing rate changes and quick variations in the signal received power during the measurement interval.

As in the IB2OB channel frequency characterization, the shape of the Doppler spectrum was evaluated to find the model that better fits the measured data. In Fig. 6 is depicted the value of the RMSE goodness of fit criterion for each fitting

function and off-body distance averaged for the entire frequencies set.

TABLE IX
MEASURED IB2OFF CHANNEL DOPPLER PARAMETERS

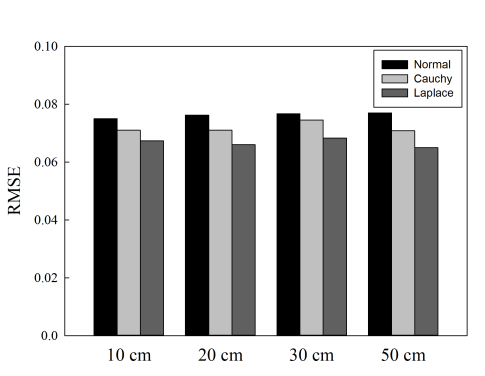| Off-body distance (cm)	f_c (GHz)	B_D (Hz)	ΔB_{Dref} (Hz)	ρ_{RMS} (Hz)
10	3.1	0.85	-0.42	0.23
	4.8	1.45	-0.73	0.39
	6	1.97	-0.65	0.58
	8.5	1.93	-0.97	0.49
20	3.1	2.17	0.90	0.56
	4.8	3.08	0.60	0.87
	6	2.53	-0.09	0.69
	8.5	1.57	-1.86	0.45
30	3.1	3.22	1.73	0.81
	4.8	3.07	0.59	0.90
	6	2.75	0.13	0.72
	8.5	3.13	-0.73	0.76
50	3.1	3.13	1.44	0.85
	4.8	2.70	0.22	0.80
	6	1.90	-1.08	0.54
	8.5	3.05	-0.81	0.83

Fig. 6. Functions RMSE goodness of fit values for every off-body distance.

As previously found, the function that better fits the shape of the measured Doppler spectrum is the Laplace one. As observed, there is little variation of the RMSE value as the off-body distance increases for any of the selected fitting functions ($\sigma < 0.02$).

C. IB2IB Radio Channel

Values of the derived Doppler parameters for the in-body to in-body channel are listed in Table X.

TABLE X
IB2IB CHANNEL DOPPLER PARAMETERS

f_c (GHz)	B_D (Hz)	ΔB_{Dref} (Hz)	ρ_{RMS} (Hz)
3.1	3.12	0.58	0.95
4.8	5.87	1.83	1.54
6	6.62	2.14	1.57
8.5	-	-	-

As already derived from Table V, the mean received power falls below the noise level for frequencies above 4.8 GHz. Thus, only the 3.1 GHz to 4.8 GHz range is practicable.

From Table X, as propagation occurs in a single medium of permittivity ε_r, measured and theoretical values of B_D are closer than in the other considered scenarios, presenting a maximum variation lower than in the rest of scenarios for the practicable band.

Finally, the shape of the Doppler spectrum was evaluated to find the model that better fits the measured data on the IB2IB channel. In Table XI the RMSE goodness of fit criterion value for each one of the three considered fitting functions is listed. Opposed to the Laplace function that was found to better describe the shape of the Doppler spectrum in the IB2OB and IB2OFF scenarios, for the IB2IB one the Normal function is the best fit. The reason can be derived from the fact that because some of the measured data are very close to the noise level and both antennas are interacting in the near field area, there exists a higher random dispersion on the measured data as the frequency increases.

TABLE XI
IB2IB DOPPLER SPECTRUM SHAPE FITTING RMSE VALUES

f_c (GHz)	Normal	Cauchy	Laplace
3.1	0.081	0.134	0.124
4.8	0.084	0.131	0.123
6	0.088	0.107	0.101
8.5	-	-	-

VII. CONCLUSIONS

This paper presents a study of the human breathing influence on the radio channel in WBAN applications, considering at least one of the communication nodes inside the body and operating at UWB frequencies. Three propagation channels have been considered: in-body to on-body (IB2OB), in-body to off-body (IB2OFF) and in-body to in-body (IB2IB). The effects in frequency of the relative movement between nodes have been addressed in terms of the Doppler spread and the Doppler spectrum shape fitting.

A simplified theoretical model of breathing, obtained by fitting the real channel measurements, has also been presented and used to derive reference values of the Doppler spread in each scenario. Reference values of B_D have been found to reasonably fit the measured ones, with variations lower than 1 Hz especially when the breathing rate keeps constant during the considered interval.

From the study of the Doppler spectrum shape fitting, the Laplace distribution is found to be the best fit for the IB2OB and IB2OFF scenarios while the Normal one is a better option for the IB2IB scenario.

Finally, because of the selected phantom presents an homogeneous propagation medium, results in real multi layer living tissues with different dielectric constants could differ, turning some of the considered frequency bands useless because of the high losses.

REFERENCES

[1] P. J. Soh, G. A. E. Vandenbosch, M. Mercuri and D. M. M. -P. Schreurs, "Wearable wireless health monitoring: Current developments, challenges, and future trends", IEEE Microw. Mag., vol. 16, no. 4, pp. 55-70, May 2015.

[2] S. Movassaghi, M. Abolhasan, J. Lipman, D. Smith and A. Jamalipour, "Wireless body area networks: a survey", IEEE Commun. Surveys Tuts., vol. 16, no. 3, pp. 1658-1686, Jan. 2014.

[3] C. C. Y. Poon, B. P. L. Lo, Mehmet Rasit Yuce, A. Alomainy and Y. Hao, "Body sensor networks: In the era of Big Data and beyond". IEEE Rev. Biomed. Eng., vol. 8, pp. 4-16, Apr. 2015.

[4] J. Andreu-Perez, D. R. Leff, H. M. D. Ip and G.-Z. Yang, "From wearable sensors to smart implants—toward pervasive and personalized healthcare", IEEE Trans. Biomed. Eng., vol. 62, no. 12, pp. 2750-2762, Dec. 2015.

[5] X. P. Li, Y. Yang and Y. Gao, "The biological channel modeling of implantable medical devices", 12th International Conference on Electrical Engineering/Electronics, Computer, Telecommunications and Information Technology (ECTI-CON), Hua Hin, Thailand, June 24-27, 2015.

[6] IEEE Standard for Local and Metropolitan Area Networks – Part 15.6 Wireless Body Area Networks (IEEE Std 802.15.6-2012).

[7] R. Chávez-Santiago, K. Sayrafian-Pour, A. Khaleghi, K. Takizawa, J. Wang and I. Balasingham, H. Li, "Propagation models for IEEE 802.15.6 standardization of implant communication in body area networks", IEEE Commun. Mag., vol. 51, no. 8, pp.80-87, Aug. 2013.

[8] A. Khaleghi, R. Chavez-Santiago and I. Balasingham, "Ultra-wideband statistical propagation channel model for implant sensors in the human chest", IET Microwaves, Antennas & Propagation, vol. 5, no. 15, pp. 1805-1812, 2011.

[9] R. Chávez-Santiago and I. Balasingham, "Ultrawideband signals in medicine", IEEE Signal Process. Mag., vol. 31, no. 8, pp. 130-136, Nov. 2014.

[10] R. Chavez-Santiago, I. Balasingham and J. Bergsland, "Ultrawideband technology in medicine: A survey", Journal of Electrical and Computer Engineering, vol. 2012, art. 716973, 2012.

[11] K. M. S. Thotahewa, J. M. Redoutè and M. Rasit Yuce, "Propagation, power absorption, and temperature analysis of UWB wireless capsule endoscopy devices operating in the human body". IEEE Trans. Microw. Theory Techn., vol. 63, no. 11, pp. 3823-1833, Oct. 2015.

[12] R. Chávez-Santiago and I. Balasingham, "Computation of the transmission frequency band for the ultra wideband capsule Endoscope", 7th International Symposium on Medical Information and Communication Technology (ISMICT), pp. 66-70, Tokio, Japan, Mar. 6-8 2013.

[13] K. M. S. Thotahewa, J. M. Redouté and M. R. Yuce, "Electromagnetic power absorption of the human abdomen from IR-UWB based wireless capsule endoscopy devices", IEEE International Conference on Ultra-Wideband (ICUWB), Sydney, Australia, Sept. 15-18, pp. 79-84, 2013.

[14] J. B. West, "Mechanics of Breathing", in Respiratory Physiology: The Essentials, 9th ed., Ed. Lippincott Williams & Wilkins, 2012, pp. 95-124.

[15] M. Fagevik Olsén, H. Lindstrand, J. L. Broberg and E. Westerdahl, "Measuring chest expansion; A study comparing two different instructions", Advances in Physiotherapy, vol. 13, no. 3, pp. 128-132, Aug. 2011.

[16] G. Shechter, C. Ozturk, J. R. Resar and E. R. McVeigh, "Respiratory motion of the heart from free breathing coronary angiograms", IEEE Trans. Med. Imag., vol. 23, no. 8, pp. 1046-1056, Aug. 2004.

[17] W. E. Garrett and D. T. Kirkendall, "Pulmonary Responses to Exercise And Training", in Exercise and Sport Science, Ed. Lippincott Williams and Wilkins, 1999, pp. 117-134.

[18] L. Petrillo, T. Mavridis, J. Sarrazin, A. Benlarbi-Delai and P. De Doncker, Experimental On-Body Fading and Breathing Doppler Characterization on Human Torso at 60 GHz, International Conference on Body Area Networks, Sep. 2014, London, United Kingdom.

[19] J. Zhou, D. Hara and T. Kobayashi, "Development of ultra wideband electromagnetic phantoms for antennas and propagation studies", First European Conference on Antennas and Propagation, Nice, France, Nov. 6-10, pp. 1-6, 2006.

[20] C. Tarin, P. Marti, L. Traver, N. Cardona, J. A. Diaz, and E. Antonino, "UWB channel measurements for hand-portable devices: A Comparative study," in 2007 IEEE 18th International Symposium on Personal, Indoor and Mobile Radio Communications, 2007, pp. 1–5.

[21] K. Pahlavan and A. H. Levesque, "Characterization of Radio Propagation", in Wireless Information Networks, 2nd ed., Ed. Wiley, 2005, pp. 53-91.

[22] T. S. Rappaport, "Mobile Radio Propagation: Small-Scale Fading and Multipath", in Wireless Communications: principles and practice, Ed. Prentice Hall, 1996, pp. 139-196.

[23] S. W. Smith, "Moving Average Filters", in Digital Signal Processing: A Practical Guide for Engineers and Scientists, 2nd ed., Ed. Newnes, 1999, pp. 277-284.